Asian Journal of Chemistry; Vol. 37, No. 3 (2025), 601-608

ASIAN JOURNAL OF CHEMISTRY

https://doi.org/10.14233/ajchem.2025.33252

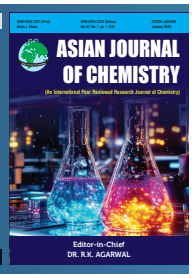

Biological Activities and Docking Simulation of Newer Dipodal Benzopyrazines based Azine Scaffold

MAROTI SUDEWAD[1], SACHIN YEOLE[2], MAHESHKUMAR JADHAV[1], SANTOSH KATHWATE[3], RAHUL MORE[4] and KUNDAN TAYADE[1,*]

[1]Department of Chemistry and Analytical Chemistry, Rajarshi Shahu Mahavidyalaya (Autonomous), Latur-413512, India
[2]Department of Chemistry, Bhusawal Arts, Science and P.O. Nahata Commerce College, Bhusawal-425201, India
[3]Department of Biotechnology, Savitribai Phule Pune University, Pune-411007, India
[4]Department of Microbiology, Dayanand Science College, Latur-413531, India

*Corresponding author: Fax: +91 2382 253645; Tel: +91 2382 245933; E-mail: kundantayade@gmail.com

Received: 23 December 2024; *Accepted*: 1 February 2025; *Published online*: 28 February 2025; AJC-21916

In this study, novel benzopyrazine-based motif 2-((2,3-*bis*(4-bromophenyl)quinoxalin-6-yl)(phenyl)-methylene)-1-((2,3-*bis*(4-bromophenyl)-quinoxalin-7-yl)(phenyl)methylene)hydrazine (compound **2**) was synthesized and characterized. Among the tested microbes, compound **2** has demonstrated potent activity against the bacterial strains *B. subtilis* and *B. megaterium* (with MICs of 31.25 and 15.62, respectively), as well as the fungal strains *R. oryzae*, *P. chrysogenum* and *A. niger* (with MICs of 31.25, 62.5 and 62.5, respectively). Compound **2** (1 mg/mL) was also found to be a potent DPPH-reducing agent as compared to ascorbic acid. *In vitro* hemolytic assay revealed negligible activity (within 5% permissible limit) as compared to positive control Triton-X 100. Molecular docking studies indicated that compound **2** binds to the GyrB ATP-binding site through hydrogen bonds, hydrophobic interactions, and π-cation interactions, demonstrating favourable *in silico* interaction energy scores. Exploration of DFT shows that HOMO & LUMO are mainly located around the benzene rings and nitrogen atoms rather than bromine.

Keywords: Benzopyrazine, Molecular docking, Biological activities, DFT studies.

INTRODUCTION

Several heterocyclic groups, including aza-, oxo-, phospho- and thio-heterocycles, as well as many pharmacologically relevant natural and synthetic compounds include nitrogen heterocycles [1]. Benzopyrazine is a fused bicyclic scaffold in which pyrazine and benzene are hybridized and also known as quinoxaline (weakly basic) [2]. Few naturally occurring antibiotics and nutrients, like riboflavin, include the benzopyrazine moiety as a key structural element [3]. The pharmacology of the benzopyrazine scaffolds (with a larger spectrum) reveals a wide range of applications in the treatment of viral, bacterial, fungal, inflammatory, cancer, diabetic and HIV disorders [4-7]. Moreover, benzopyrazine can be used to make fluorescence sensors, photovoltaic materials and other things [8-11].

The increasing prevalence of drug-resistant bacteria and the introduction of novel diseases has created a persistent demand for the synthesis of innovative heterocyclic compounds as prospective therapeutic agents [12]. Topoisomerases are bacterial enzymes that play a key role in relaxing super-coiling of DNA during DNA replication. Clinical trials have shown that these enzymes are effective targets for the development of novel antibacterial agents [13]. The enzymes involved play a vital role in the mechanisms of DNA replication, repair and decatenation, as they induce a change in the topological configuration of DNA. Consequently, these enzymes play a crucial role in the viability of cells. Type IIA topoisomerase enzymes are present in bacteria and play a crucial role in the gyrase reaction [14]. The temporary separation of the DNA strands is one of the activities catalyzed by enzyme. DNA gyrase plays a critical role in the replication process by promoting the formation of negative supercoiling in DNA. The four sub-units that make up DNA gyrase form a heterotetramer. DNA gyrase is composed of four proteins, two GyrA and two GyrB (A2B2). DNA gyrase catalyzes a series of highly intricate reactions during DNA replication, allowing for a wide range of potential therapeutic

interventions. Clinically significant classes of antibacterial drugs, such as fluoroquinolones, target gyrase enzymes; these drugs interact primarily with GyrA subunits to stabilize the enzyme-DNA complex, while aminocoumarins (*e.g.* novobiocin and clorobiocin) bind to GyrB use, prompting the search for new inhibitor classes that target different enzyme binding sites to prevent the development of cross-resistance [15].

Herein, the synthesis of 2-((2,3-*bis*(4-bromophenyl)quinoxalin-6-yl)(phenyl)methylene)-1-((2,3-*bis*(4-bromophenyl)-quinoxalin-7-yl)(phenyl)methylene)hydrazine (**2**) was carried out as part of our interest in the synthesis of hydrazine-based derivatives. Additionally, the quantum chemical computations of compound utilizing (DFT) as well as investigations on cytotoxicity, antimicrobials, antioxidants and molecular docking have all been conducted.

EXPERIMENTAL

The required chemicals were bought from Sigma-Aldrich and used without further purification. The FT-IR spectra was captured from Shimadzu FTIR spectrophotometer (Thermo Fischer Scientific, Nicolet-iS10) using KBr pellets in the 4000-400 cm^{-1} range. ^1H NMR and ^{13}C NMR spectra were captured using a Bruker AVANCE-500 (400 MHz) spectrometer using $CDCl_3$ as a solvent. Shimadzu UV-visible spectrophotometer (UV-1700 Pharma Spec) was used to record the UV-visible spectra.

Synthesis of 2-((2,3-*bis*(4-bromophenyl)quinoxalin-6-yl)(phenyl)methylene)-1-((2,3-*bis*(4-bromophenyl)quinoxalin-7-yl)(phenyl)methylene)hydrazine (2): In first step, 4,4′-dibromobenzil (0.368 g, 1 mmol) was added to a magnetically agitated solution of 3,4-diaminobenzophenone (0.212 g, 1 mmol) in presence of 10 mL glacial acetic acid and then refluxed for 3 h. An off-white solid of (2,3-*bis*(4-bromophenyl)-quinoxalin-7-yl)(phenyl)methanone (**1**) was obtained, when the reaction mixture was poured over crushed ice. Compound **1** was filtered, vacuum-dried and then recrystallized with ethanol [16]. Afterwards, hydrazine hydrate (0.050 g, 1 mmol) in ethanol was added to a magnetically stirred compound **1** solution (1.088 g, 2 mmol) and the resulting reaction mixture was left to stir at room temperature for 4 h leading to obtain compound **2** (**Scheme-I**). Yield: 92%, m.p.: > 250 ºC; FTIR (nujol mull, cm^{-1}): 3063.64, 1899.44, 1652.00, 1595.80, 1585.66, 1488.90, 1445.97, 1405.11, 1390.12, 1332.75, 1317.73, 1297.33, 1158.38, 1136.30, 976.96, 915.58 ; ^1H NMR (400 MHz, DMSO-d_6) δ ppm: 8.279-8.283 (t, 2H,Ar-H, *J* = 8 Hz), 7.51-7.56 (m, 2H, Ar-H), 7.655-7.659 (t, 1H, Ar- H, *J* = 8 Hz), 8.513 (s, 1H, Ar-H), 7.445-7.462 (d, 1H, Ar-H, *J* = 6.8 Hz), 7.405-7.422 (d, 1H, Ar-H, *J* = 6.8 Hz), 7.441-7.457 (d, 2H, Ar-H, *J* = 6.4 Hz), 7.530-7.546 (d, 2H, Ar-H, *J* = 6.4 Hz), 7.897-7.915 (d, 2H, Ar-H, *J* = 7.2 Hz), 7.522-7. 540 d, 2H, Ar-H, *J* = 7.2 Hz); ^{13}C NMR (75 MHz, $CDCl_3$) δ ppm: 195.54 (C=N), 153.53 (Ar C=C), 153.00, 142.87, 140.20, 138.67, 137.20,137.17, 137.02, 132.92, 132.47, 132.25, 131.77, 131.45, 131.34, 130.26, 130.11, 129.67,

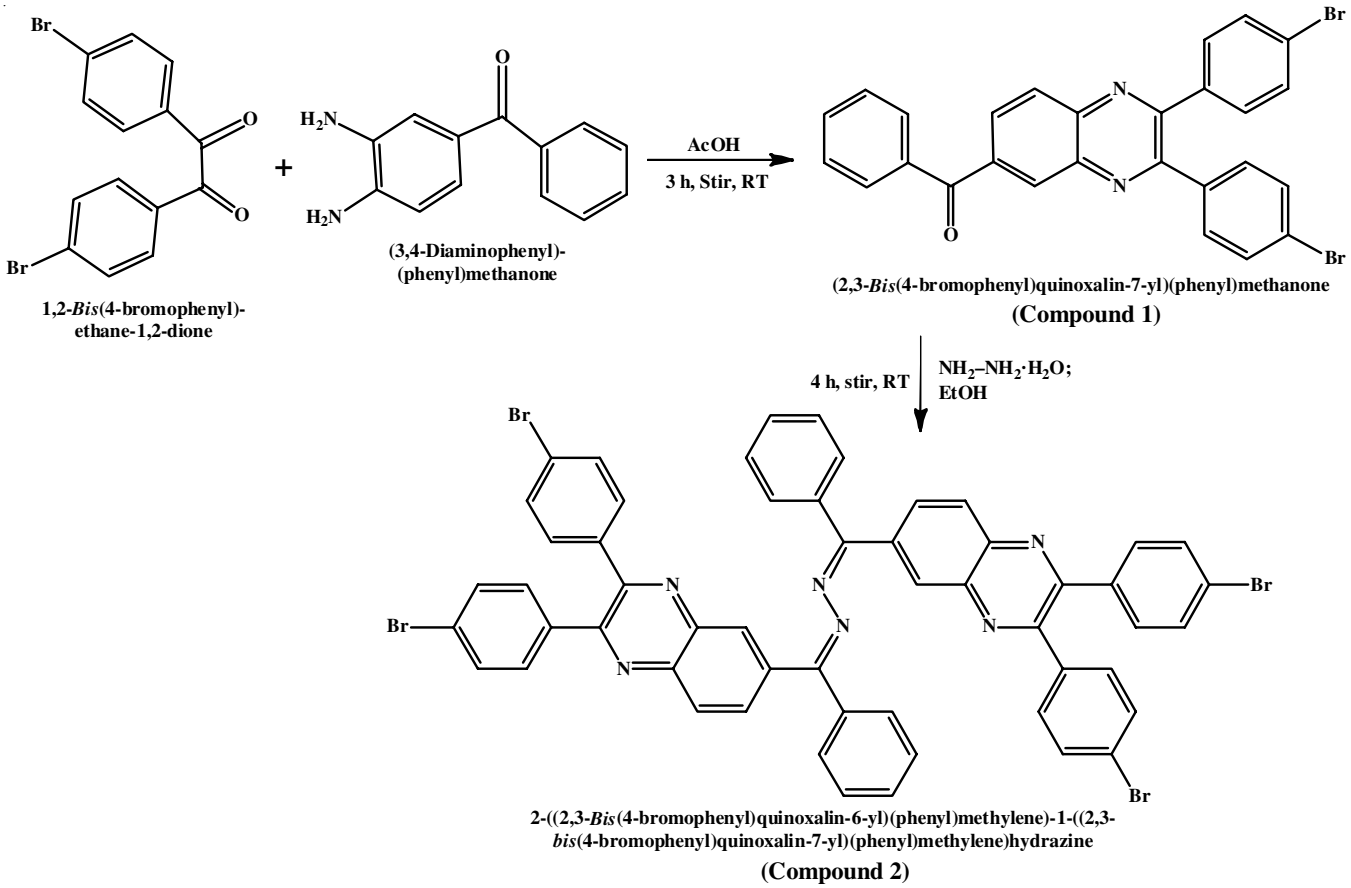

Scheme-I: Syntheses of compounds **1** and **2**

128.54, 124.26, 124.09; ESI-MS (*m/z*), [$C_{54}H_{32}Br_4N_6$+Na^++H^+], calculated: 1108.486, found: 1108.901.

Theoretical computations: Density functional theory (DFT) was used to perform the quantum chemical calculations for compound **2** and computational Gaussian16 was used for the theoretical computations [17]. The geometry optimizations of compound **2** was performed using the DFT method with Becke's three-parameter hybrid exchange–correlation functional (B3LYP) [18,19] and the 6-311++G(d,p) basis set in the gas phase.

Antimicrobial activity: According to the reported methodology [20,21], the antibacterial potential of compound **2** was evaluated by disk diffusion assay. In brief, the dried paper disk (Whatman filter paper No. 1) containing compound **2** (0.001 mM) was placed on the surface of the sterile solidified nutrient agar/potato dextrose agar plates, which were spread with inoculums of microbial cultures (0.5 McFarland standard) as per CLSI standards. Streptomycin and fluconazole were used as a standard (0.001 mM). The plates were incubated at 30 ºC for 24 h after being refrigerated for 1 h to facilitate diffusion. After incubation, the zones around the discs were measured by the zone scale (Himedia Pvt. Ltd., Mumbai, India).

Resazurin microtiter assay (REMA): According to the previously described protocol [20-22], the REMA plate analysis was carried out. In brief, 100 µL of Middlebrook 7H9-S (containing 0.1% casitone, 0.5% glycerol and supplemented with oleic acid, albumin, dextrose and catalase) broth medium was dispensed in each well of a sterile flat-bottom 96-well plate and serial two-fold dilutions of the synthesized compound was prepared directly in the plate. Inoculums (100 µL) were added to each well. Sterile cold water was added to all perimeter wells to avoid evaporation during incubation. The plate was covered, sealed in a plastic bag and incubated at 37 ºC for 24 h. After incubation, 30 µL of resazurin solution (0.01% in sterile deionized water) was added to each well and the plate was re-incubated for 4 h. The MIC was established as the lowest drug concentration that prevented the colour change from blue to pink, which indicated the development of bacteria. The reference standard and the synthesized compound drug concentration ranges were 0.048-500 µg/mL. The assay was performed in triplicate.

Determination of antioxidant activity

DPPH radical scavenging assay: The experiment was carried out by mixing equal amounts of DPPH and the synthesized compound **2**, resulting in a final volume of 3 mL. After incubating the samples for 20 min, the absorbance at 517 nm was measured. Ascorbic acid was utilized as standard. Compound **2** and standard concentrations both were kept at 1 mM [21-23].

$$\text{Radical scavenging activity (\%)} = 1 - \frac{T}{C} \times 100$$

Antioxidant activity by hydroxyl radical assay: The $^{\bullet}OH$ radical scavenging activity was demonstrated with a Fenton reaction. The protocol involves the typical reaction mixture containing 60 µL of $FeCl_2$ (1 mM), 90 µL of 1,10-phenanthroline (1 mM) and 2.4 mL of phosphate buffer (0.2 M, pH 7.8), 150 µL of H_2O_2 (0.17 M) and 1.5 mL of compound **2** (1 mM). The reaction commenced with the addition of H_2O_2. After 5 min incubation at room temperature, the absorbance was recorded at 560 nm and ascorbic acid (1 mM) was used as a reference [21,22].

Cell cytotoxicity assay: Using human red blood cells, as indicated earlier, the hemolytic activities of the synthesized compound were evaluated. Initially, 5 mL of human blood was drawn into tubes containing 1 mg of EDTA as anticoagulant. Centrifugation (Remi, India) was used to separate the erythrocytes for 10 min at 1600 × g at 20 ºC. Three PBS washes were performed on the obtained pellet. Next, 10% (v/v) erythrocyte suspension in PBS was made. PBS was used to prepare a 1:10 dilution from this 10% solution, which was then used for the assay. The protocol involves the addition of 100 µL of erythrocytes suspension to the tube containing the synthesized compound 100 µL (50 µg/mL) and Triton X 100 (0.001 N) was used as a reference. The tubes were incubated for 1 h at 37 ºC and centrifuged at the same conditions mentioned above. From supernatant fluid, 150 µL was transferred to flat bottom 96 well microtiter plate (BD falcon, USA) and the absorbance was measured at 540 nm by using Thermo make automated microplate reader. Hemolysis (%) was calculated using the following equation:

$$\text{Hemolysis (\%)} = \frac{A - B}{C - B} \times 100$$

where, A = A_{450} of test compound treated sample, B = A_{450} of buffer treated sample; C = A_{450} of Triton X-100 treated sample.

Molecular modelling: Calculations of molecular docking were carried out using AutodockVina [24] and UCFS Chimera was used as the interface [25]. The DNA gyrase B ATP-binding domain crystal structures from *E. coli* were obtained from the Brookhaven Protein Data Bank. Introduction for 4DUH in the PDB [26-28]. For the purpose of locating hydrogen bonds and hydrophobic interactions between residues at the active site, the software packages LigPlot +1.4 [29] and AutoDocktools 1.5.6/AutoDock 4.2 [30] were utilized for docking flexible ligands into the rigid enzyme model. In case of the DNA gyrase B ATP-binding domain found in *E. coli*, the grid size was determined to be 40 × 40 × 40 points, with a grid spacing of 0.503 Å and the grid centre was positioned at dimensions (x, y, z: 3.151, 2.814, 38.950). In order to find the optimal parameter settings, the genetic algorithm was utilized and the number of runs was set to 50. The following is a list of the parameters that govern the docking procedure: population size of 300, the maximum number of energy assessments per cycle analysis of 2.5×10^7, generation of 50 mating receptor conformations for the ligand, clusters maintained a root mean square deviation (RMSD) of 2.0 Å and all other parameters were left at their default settings. Compound **2** and ligand structures were drawn and converted into canonical SMILES in ChemDraw. Open-Babel software was used to convert the canonical SMILES to PDBQT format of compound **2** and same was used for docking purposes at AutoDocktool 1.5.6.

UCFS Chimera and Auto-Dock tools 1.5.6 were used to analyze and represent the 3D rendering of complex enzyme–

ligand, as well as the conformer with the best docking energy and interactions with amino acid residues. The position of the conserved residues was obtained directly from the high resolution X-ray crystal structures (resolution 2.1 Å) of the DNA gyrase B ATP-binding domain from *E. coli* (PDB: 4DUH). Redocking was carried out so that it could be established whether or not the predicted poses of the two protein complexes were accurate. When compared to the experimentally determined co-crystallized binding pose, the predicted docking poses showed an RMSD value of 1.0 (4DUH), which is considered to be very close.

RESULTS AND DISCUSSION

Based on the ^{1}H NMR, ^{13}C NMR, mass and IR spectra, the results were consistent with the structure of compound **2**. The FT-IR spectrum of **2** showed characteristic peaks at 3064 cm^{-1} (-C-H) stretching, 1652 and 1586 cm^{-1} for –C=N of quinoxaline and hydrazine, respectively and 1596 cm^{-1} (-C=C- of C_6H_5 ring). The ^{1}H NMR spectrum depicted the chemical shift peaks between δ 7.266-8.315 ppm, which confirmed the structure of compound **2**. The mass spectra indicated a formation of the $[M+H+Na]^+$ peak at 1108.486 for 4×(^{79}Br), at 1110.903 for 2×(^{79}Br &^{81}Br) and at 1112.907 for 4×(^{81}Br).

DFT studies: The optimized structure of compound **2** at B3LYP/6-311++G(d,p) level is shown in Fig. 1. The DFT studies revealed that the benzene rings and the nitrogen atoms are the principal locations of LUMO, which has a value of -0.10333 a.u. (Fig. 2). Around nitrogen atoms, there is a high concentration of electrons. HOMO is situated on the bromine atoms, which are primarily positioned around the benzene rings and nitrogen atoms and have a value of -0.23248 a.u. It was found that the HOMO-LUMO gap is 0.12915 au corresponding to 3.51 eV. HOMO and LUMO levels of the as-synthesized heterocyclic molecule revealed the isosurface value of 0.025 a.u. The isosurface of electrostatic potential revealed with value -0.025 a.u. with electron density concentrated around nitrogen atoms (Fig. 3).

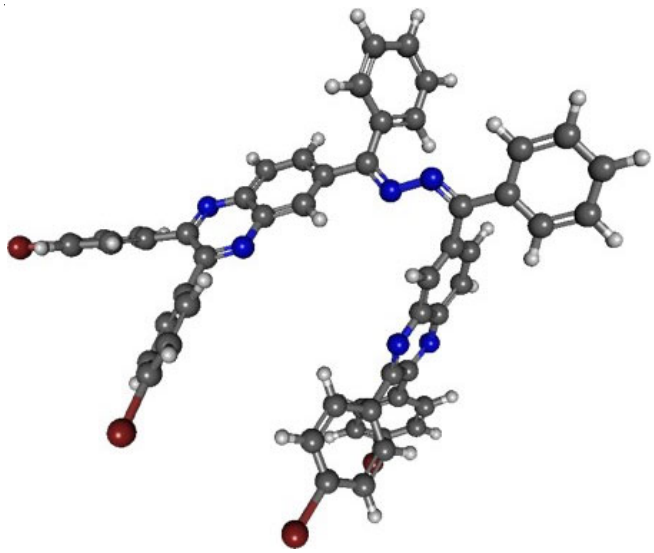

Fig. 1. Structure of compound **2** optimized at B3LYP/6-311++G(d,p) level of theory

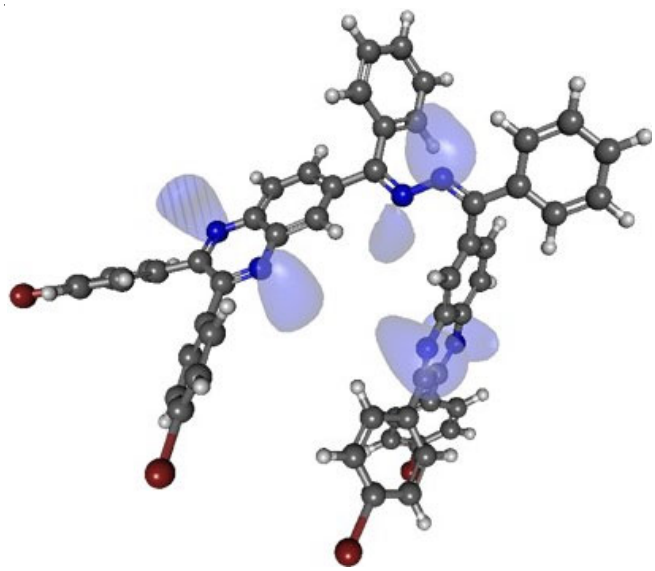

Fig. 3. Isosurface of electrostatic potential with value -0.025 au and electron density concentrated around nitrogen atoms

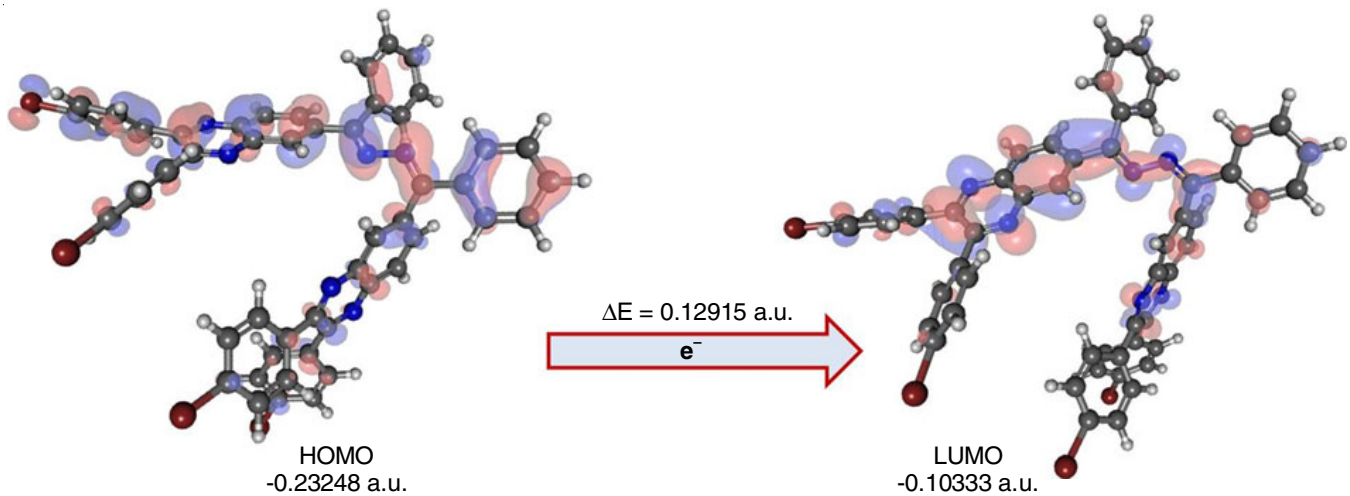

Fig. 2. DFT computed isosurfaces of HOMO and LUMO of compound **2** with value 0.025 a.u.

Antimicrobial activities

Disc diffusion assay: The threat of increasing antibiotic resistance among bacterial and fungal pathogens demands the development of novel and reliable synthetic compounds with low to zero toxicity. The antibacterial and antifungal screening assay was performed by disc diffusion method and results are summarized in Table-1. The results indicated that the compound **2** exhibited synergistic inhibition.

Resazurin microtiter plate assay (REMA): For checking the minimum inhibitory concentration (MIC) and fungal inhibitory concentration (FIC), one of the proficient methods, REMA assay was used. The oxidation-reduction mechanism is involved in the resazurin assay and it is a simple, inexpensive method that is routinely used in checking cellular viability. The basic mechanism involves the reduction of blue colour to pink by the metabolically active live cells. No change in blue colour indicates a total absence of metabolically live cells. The MIC and FIC values of the synthesized compounds were evaluated, and the results shown in Table-2 clearly highlight the varying sensitivity of pathogens to the test compounds of interest. The results are expressed as the mean values of three independent experiments.

Antioxidant activities: The results (Fig. 4) demonstrated that the synthesized compound **2** (1 mg/mL) exhibited significant DPPH reducing capabilities, exhibiting a comparable scavenging potential to that of ascorbic acid. When compared to α-tocophero, compound **2** has demonstrated a promising ability to scavenge •OH radicals.

Hemolytic activity: The hemolytic potential of synthesized compound **2** towards the host cell was calculated by *in vitro* assay of hemolytic activity. The results (Fig. 5) revealed that the tested synthesized compound **2** exhibits negligible hemolytic activity as compared to the positive control Triton X-100 and was within the permissible limit of 5% hemolysis.

Molecular modelling study: Docking studies were conducted on the compound that was synthesized in order to make a prediction about their affinity to the bacterial protein DNA GyrB that was produced by *E. coli.* A conserved cavity was located in the immediate vicinity of ligands at the protein-binding site and the binding modes were then predicted using conserved amino acid residues. The least energy-binding mode for the ligand–protein complex, also known as the top-ranked

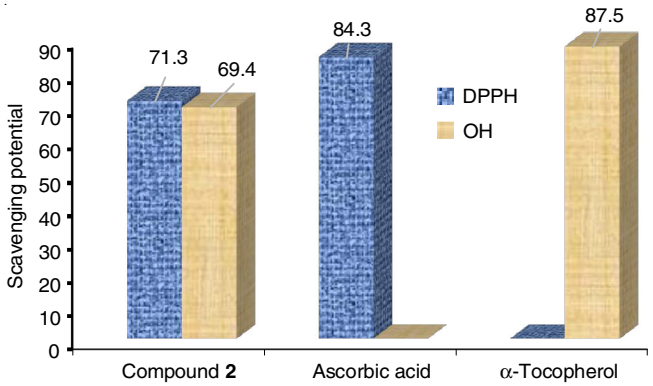

Fig. 4. Antioxidant potential of synthesized compound **2** compared to standards

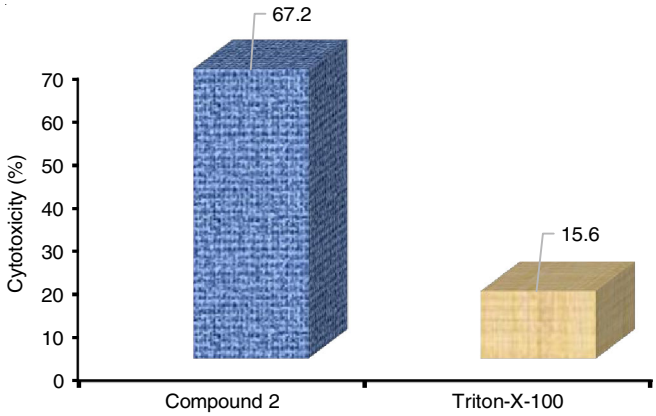

Fig. 5. % Cytotoxicity profile of synthesized compound **2** compared to standard Triton X-100

TABLE-1
ZONE OF INHIBITION OF SYNTHESIZED COMPOUNDS AGAINST SOME PATHOGENIC MICROORGANISMS

Compound	Zone of inhibition against pathogenic microorganisms							
	Bacterial strains				Fungal strains			
	E. coli	*B. subtilis*	*B. megaterium*	*S. aureus*	*R. oryzae*	*P. chrysogenum*	*A. niger*	*C. albicans*
Compound **2**	++	+++	+++	+++	++	+++	+++	+
Streptomycin		+++	+++	+++	+++	NA	NA	NA
Flucanozole		NA	NA	NA	NA	+++	+++	+++

+ = < 5mm zone, ++ = 5-10 mm zone, +++ = 11-15 mm zone, ++++ = >16 mm zone, NA = Not applicable

TABLE-2
THE MIC AND FIC OF SYNTHESIZED COMPOUNDS AGAINST SOME PATHOGENIC MICROORGANISMS

Compound	MIC against pathogenic microorganisms							
	Bacterial strains				Fungal strains			
	E. coli	*B. subtilis*	*S. typhi*	*S. aureus*	*R. oryzae*	*P. chrysogenum*	*A. niger*	*C. albicans*
Compound **2**	125	62.5	62.5	31.25	125	62.5	62.5	500
Streptomycin	3.9	1.95	3.9	3.9	NA	NA	NA	NA
Flucanozole	NA	NA	NA	NA	3.9	3.9	3.9	7.81

NA = Not applicable

solution, was examined for the possibility of interactions with the amino acid residues that make up the ATP-binding site. In particular, the hydrogen bond interactions that are provided by the highly conserved amino acids, like Aps73 Gly77, Gly 101 and Thr165 (PDB: 4DUH), were taken into consideration as depicted in Fig. 6.

An investigation into the docking poses of compound **2** revealed that all poses occupy the same region of DNA gyrase B ATP-binding pocket [31] and exhibit favourable *in silico* interaction energy scores (Table-3). In order to bind the ligand to the receptor, it was thought that hydrogen bonds were established between the ligand and the conserved amino acid residues. Compound **2**, which were virtually analyzed to be an inhibitor of DNA gyrase, have values that are consistent with standard DNA gyrase inhibitors and the MICs that were obtained through experimentation. Fig. 6a shows the binding mode for compound **2** within the context of the ATP-binding site. The stereo view of the docked complex primarily reveals the formation of a direct hydrogen bond between the hydrogen of N5 nitrogen of the quinoxaline ring and the Arg136 residue, while the hydrogen of the N2 nitrogen of the quinoxaline ring interacts with the conserved Gly101 (Fig. 6b). These three H-bonds, with lengths of 2.65, 3.29 and 2.57 Å, respectively, form a pattern of hydrogen bond donor–acceptor interaction, which is representative of the vast majority of DNA gyrase inhibitors [24-26]. This pattern is considered to be of the utmost importance and appears to be absolutely necessary [32]. In addition to forming hydrogen bonds, compound **2** also engages in the hydrophobic interactions with the residues ARG(76), ILE(78), PRO(79), ALA(90), ILE(94), LYS(103), VAL(120) and THR(163), which are located in the hydrophobic pocket that is a part of the ATP-binding site. In addition, compound **2** also forms π-cation bonds with some other conserved amino acids like Arg132 and Lys103. The calculated binding free energy and inhibition constant (K_d) for the compound **2** are –9.51 kcal/mol and 106.50 nM, respectively (Table-3).

TABLE-3
INHIBITION CONSTANT (K_d) AND BINDING ENERGY COMPOUND **2** AND THE STANDARD GYRASE B INHIBITORS CALCULATED BY AUTO-DOCK TOOLS 1.5.6

Compounds	Inhibition constant (K_d)	Free energy of binding (Kcal/mol)
Cyclothialidine	6600 nM	NA
Clorobiocin	1.2 nM	–12.2
Novobiocin	1200 nM	–10.1
Compound **2**	106.50 nM	–9.51

Interactions obtained after docking the compound **2** in conserved pocket of the ATP bind region of gyrase B were consistent with that of interactions of standard inhibitors like cyclothialidine clorobiocin and novobiocin with some changes. The modifications involve novel interacting moieties and the characteristics of the bond. The hydrophobic interactions provide stability to the complex and the more the interaction stable will be the complex [33]. In case of standard inhibitors, four to five hydrophobic amino acids are involved in the interactome. On the other hand, compound **2** has eight new and most of highly hydrophobic amino acids compared to standard inhibitors. PRO(79) and ILE(94) are the conserved hydrophobic interaction and additionally compound **2** interacted with ARG (76), ILE(78), ALA(90), LYS(103), VAL(120), THR(163) hydrophobic amino acids forming more stable receptor-ligand complex. The π-cation interactions are also conserved by compound **2** with three-bound formation providing more stability to the complex. Furthermore, compound **2** shares similarities in the range of distances of various bonds. The distance ranges of

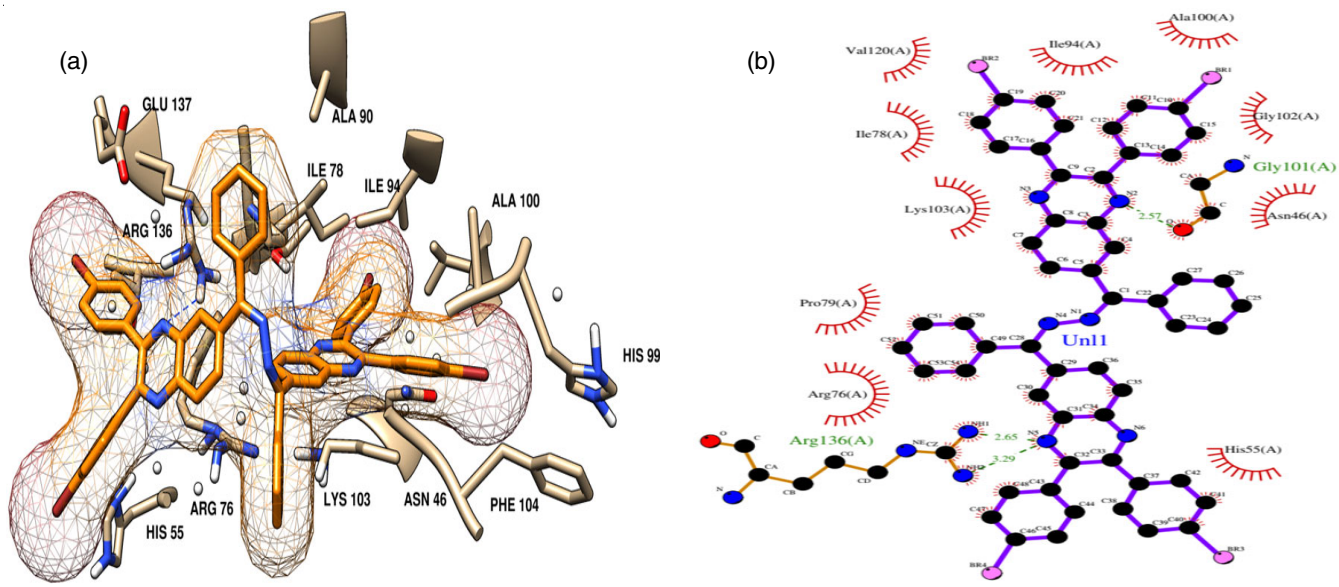

Fig. 6. Molecular docking interaction of compound **2** with PDB: 4DUH determined by Autodock 4.2 (a) compound **2** docked in orange colour stick style and PDB: 4DUH receptorResidues are in offwhite and ribbon and stick style. Various amino acids are labelled in three-lettercodesand numbers in the peptide chain (displayed in UCSF chimera) (b) Various interactions of compound **2** (purple/black ball and stick) with receptors residues in red bumps and hydrogen bond interaction as yellow/black/blue/red ball and stick with a green dotted line as hydrogen bond (displayed in LigPlot+ 1.4)

TABLE-4
BINDING INTERACTION OF MS1, CYCLOTHIALIDINE, CLOROBIOCIN AND NOVOBIOCIN TOWARDS DNA GYRASE (4DUH): AA-THREE LETTER CODE FOR AMINO ACIDS AND NUMBER IN THE PEPTIDE CHAIN

Hydrophobic interactions		Hydrogen bond		π-Cation interactions		Water bridges		Salt bridges	
AA (number)	Distance	AA (number)	Distance	AA (number)	Distance	AA (number)	Distance	AA (number)	Distance
Compound **2**									
ARG(76)	3.97	ARG(136)	2.65	ARG(76)	5.28	–	–	–	–
ILE(78)	3.14	ARG(136)	3.29	ARG(76)	5.25	–	–	–	–
PRO(79)	3.04	GLY(101)	2.57	LYS(103)	4.19	–	–	–	–
ALA(90)	3.9	–	–	–	–	–	–	–	–
ILE(94)	3.46	–	–	–	–	–	–	–	–
LYS(103)	3.25	–	–	–	–	–	–	–	–
VAL(120)	3.5	–	–	–	–	–	–	–	–
THR(163)	3.94	–	–	–	–	–	–	–	–
Cyclothialidine									
VAL(43)	3.39	ASP(73)	1.89	LYS(103)	4.48	ARG(136)	2.99	ARG(76)	4.35
ALA(47)	4	GLY(101)	1.83	–	–	–	–	–	–
GLU(50)	3.74	THR(165)	2.99	–	–	–	–	–	–
PRO(79)	3.53	–	–	–	–	–	–	–	–
VAL(167)	3.78	–	–	–	–	–	–	–	–
Clorobiocin									
VAL(43)	3.78	ASN(46)	3.1	ARG(76)	3.64	GLY(75)	4.09	ARG(76)	3.9
ASN(46)	3.77	ASN(46)	2.07	ARG(76)	4.04	ARG(76)	3.34	ARG(136)	3.79
Val(71)	3.98	–	–	–	–	ARG(136)	2.52	–	–
PRO(79)	3.97	–	–	–	–	ARG(136)	3.26	–	–
ILE(90)	3.7	–	–	–	–	–	–	–	–
Novobiocin									
PRO(79)	3.8	ASN(46)	2.02	ALA(47)	3.11	ARG(76)	4.03	ARG(76)	4.03
PRO(79)	3.72	ASP(73)	1.94	ARG(76)	4.04	ARG(76)	3.76	–	–
ILE(94)	3.94	THR(165)	3.03	ARG(76)	2.7	–	–	–	–
ILE(94)	3.73	–	–	ARG(76)	4.01	–	–	–	–

hydrophobic bonds are from 3.39 to 4.0 Å, 3.70 to 3.98 Å, 3.72 to 3.94 Å and 3.04 to 3.94 Å for cyclothialidine, clorobiocin, novobiocin and compound **2**, respectively. In case of hydrogen bonds, the distance ranges are 1.83 to 2.99 Å, 2.07 to 3.10 Å, 2.02 to 3.03 Å and 2.57 to 3.65 Å for cyclothialidine, clorobiocin, novobiocin and compound **2** respectively. Although the π bond distances for compound **2** are higher than other standard inhibitors, the number of bonds is more and eventually balances the stability provided by π bonds compared with standard inhibitors (Table-4).

Conclusion

In conclusion, a novel dipodal heterocyclic macromolecule compound **2** based on benzopyrazine as well as hydrazine core were synthesized and optimized its DFT computed structure. The antioxidant activity using antimicrobial assay, DPPH and OH radicals assay and cytotoxicity study revealed the high biological applicability of compound **2**. The docking results showed that the studied ligands reach the GyrB ATP-binding site under hydrogen bond and hydrophobic interactions along with the π-cation interactions, exhibiting favourable *in silico* interaction energy scores. These findings are based on the 3D structure of DNA GyrB and the structural similarity in the binding site and modality of compound **2** with known GyrB inhibitors.

CONFLICT OF INTEREST

The authors declare that there is no conflict of interests regarding the publication of this article.

REFERENCES

1. M.M. Heravi and V. Zadsirjan, *RSC Adv.*, **10**, 44247 (2020); https://doi.org/10.1039/d0ra09198g
2. A.R. Katritzky and B.V. Rogovoy, *Chem. Eur. J.*, **9**, 4586 (2003); https://doi.org/10.1002/chem.200304990
3. J. Rock, D. Garcia, O. Espino, S.A. Shetu, M.J. Chan-Bacab, R. Moo-Puc, N.B. Patel, G. Rivera and D. Bandyopadhyay, *Front. Chem.*, **9**, 725892 (2021); https://doi.org/10.3389/fchem.2021.725892
4. V. Montero, M. Montana, M. Carré and P. Vanelle, *Eur. J. Med. Chem.*, **271**, 116360 (2024); https://doi.org/10.1016/j.ejmech.2024.116360
5. M. Tristán-Manzano, A. Guirado, M. Martínez-Esparza, J. Gálvez, P. García-Peñarrubia and A.J. Ruiz-Alcaraz, *Curr. Med. Chem.*, **22**, 3075 (2015); https://doi.org/10.2174/0929867322666150812144104
6. I. Briguglio, S. Piras, P. Corona, E. Gavini, M. Nieddu, G. Boatto and A. Carta, *Eur. J. Med. Chem.*, **97**, 612 (2015); https://doi.org/10.1016/j.ejmech.2014.09.089
7. M.F. Zayed, *Chemistry*, **5**, 2566 (2023); https://doi.org/10.3390/chemistry5040166
8. J. Yuan, J. Ouyang, V. Cimrová, M. Leclerc, A. Najari and Y. Zou, *J. Mater. Chem. C Mater. Opt. Electron. Devices*, **5**, 1858 (2017); https://doi.org/10.1039/C6TC05381E
9. J.-Y. Jaung, *Dyes Pigments*, **71**, 245 (2006); https://doi.org/10.1016/j.dyepig.2005.07.008
10. M.B. Desta, N.S. Vinh, C. Pavan Kumar, S. Chaurasia, W.T. Wu, J.T. Lin, T.C. Wei and E.W.-G. Diau, *J. Mater. Chem. A*, **6**, 13778 (2018); https://doi.org/10.1039/C8TA04774J
11. M.L. Jiang, J.J. Wen, Z.M. Chen, W.H. Tsai, T.C. Lin, T.J. Chow and Y.J. Chang, *ChemSusChem*, **12**, 3654 (2019); https://doi.org/10.1002/cssc.201900505
12. O.O. Ajani, *Eur. J. Med. Chem.*, **85**, 688 (2014); https://doi.org/10.1016/j.ejmech.2014.08.034

13. N. Malpathak and S. Baikar, *Pharmacogn. Rev.*, **4**, 12 (2010); https://doi.org/10.4103/0973-7847.65320
14. J. Hirsch and D. Klostermeier, *Nucleic Acids Res.*, **49**, 6027 (2021); https://doi.org/10.1093/nar/gkab270
15. K. Tayade, G.-S. Yeom, S.K. Sahoo, H. Puschmann, S.B. Nimse and A. Kuwar, *Antioxidants*, **11**, 2138 (2022); https://doi.org/10.3390/antiox11112138
16. D.N. Kanekar, S. Chacko and R.M. Kamble, *Dyes Pigments*, **167**, 36 (2019); https://doi.org/10.1016/j.dyepig.2019.04.005
17. M.J. Frisch, G.W. Trucks, H.B. Schlegel, G.E. Scuseria, M.A. Robb, J.R. Cheeseman, G. Scalmani, V. Barone, G.A. Petersson, H. Nakatsuji, X. Li, M. Caricato, A.V. Marenich, J. Bloino, B.G. Janesko, R. Gomperts, B. Mennucci, H.P. Hratchian, J. V. Ortiz, A. F. Izmaylov, J. L. Sonnenberg, D. Williams-Young, F. Ding, F. Lipparini, F. Egidi, J. Goings, B. Peng, A. Petrone, T. Henderson, D. Ranasinghe, V. G. Zakrzewski, J. Gao, N. Rega, G. Zheng, W. Liang, M. Hada, M. Ehara, K. Toyota, R. Fukuda, J. Hasegawa, M. Ishida, T. Nakajima, Y. Honda, O. Kitao, H. Nakai, T. Vreven, K. Throssell, J.A. Montgomery Jr., J.E. Peralta, F. Ogliaro, M.J. Bearpark, J.J. Heyd, E.N. Brothers, K.N. Kudin, V.N. Staroverov, R. Kobayashi, J. Normand, K. Raghavachari, T.A. Keith, A.P. Rendell, J.C. Burant, S.S. Iyengar, J. Tomasi, M. Cossi, J.M. Millam, M. Klene, C. Adamo, R. Cammi, J.W. Ochterski, R.L. Martin, K. Morokuma, O. Farkas, J.B. Foresman and D.J. Fox, Gaussian, Inc., Wallingford CT, Gaussian 16, Revision C.01 (2016).
18. A.D. Becke, *J. Chem. Phys.*, **98**, 5648 (1993); https://doi.org/10.1063/1.464913
19. C. Lee, W. Yang and R.G. Parr, *Phys. Rev. B Condens. Matter*, **37**, 785 (1988); https://doi.org/10.1103/PhysRevB.37.785
20. R.A. More, G.B. Sanap, M.A. Karale, Y.P. Sarnikar and R.N. Gacche, *Indian J. Public Health Res. Dev.*, **11**, 607 (2020); https://doi.org/10.37506/ijphrd.v11i6.9848
21. K.B. Gangurde, R.A. More, V.A. Adole, D.S. Ghotekar, *Results Chem.*, **7**, 101380 (2024); https://doi.org/10.1016/j.rechem.2024.101380
22. G. Mandawad, R. Kamble, S. Hese, R. More, R. Gacche, K. Kodam and B. Dawane, *Med. Chem. Res.*, **23**, 4455 (2014); https://doi.org/10.1007/s00044-014-1016-y
23. R.K. Jadhav, S.S. Mahurkar, R.A. More and D.R. Munde, *J. Synth. Chem.*, **1**, 116 (2022); https://doi.org/10.22034/jsc.2022.155285
24. O. Trott and A.J. Olson, *J. Comput. Chem.*, **31**, 455 (2010); https://doi.org/10.1002/jcc.21334
25. E.F. Pettersen, T.D. Goddard, C.C. Huang, G.S. Couch, D.M. Greenblatt, E.C. Meng and T.E. Ferrin, *J. Comput. Chem.*, **25**, 1605 (2004); https://doi.org/10.1002/jcc.20084
26. M. Brvar, A. Perdih, M. Renko, G. Anderluh, D. Turk and T. Solmajer, *J. Med. Chem.*, **55**, 6413 (2012); https://doi.org/10.1021/jm300395d
27. D. Lafitte, V. Lamour, P.O. Tsvetkov, A.A. Makarov, M. Klich, P. Deprez, D. Moras, C. Briand and R. Gilli, *Biochemistry*, **41**, 7217 (2002); https://doi.org/10.1021/bi0159837
28. G.A. Holdgate, A. Tunnicliffe, W.H. Ward, S.A. Weston, G. Rosenbrock, P.T. Barth, I.W. Taylor, R.A. Pauptit and D. Timms, *Biochemistry*, **36**, 9663 (1997); https://doi.org/10.1021/bi970294+
29. R.A. Laskowski and M.B. Swindells, *J. Chem. Inf. Model.*, **51**, 2778 (2011); https://doi.org/10.1021/ci200227u
30. G.M. Morris, R. Huey, W. Lindstrom, M.F. Sanner, R.K. Belew, D.S. Goodsell and A.J. Olson, *J. Comput. Chem.*, **30**, 2785 (2009); https://doi.org/10.1002/jcc.21256
31. N.M. Irmi, B. Purwono and C. Anwar, *Indonesian Journal of Chemistry*, **21**, 1337 (2021); https://doi.org/10.22146/ijc.64428
32. G.S. Bisacchi and J.I. Manchester, *ACS Infect. Dis.*, **1**, 4 (2015); https://doi.org/10.1021/id500013t
33. C.N. Pace, H. Fu, K.L. Fryar, J. Landua, S.R. Trevino, B.A. Shirley, M.M. Hendricks, S. Iimura, K. Gajiwala, J.M. Scholtz and G.R. Grimsley, *J. Mol. Biol.*, **408**, 514 (2011); https://doi.org/10.1016/j.jmb.2011.02.053